PNAS
www.pnas.org

Supplementary Information for

Asymmetric division yields progeny cells with distinct modes of cell cycle-dependent chromosome methylation

Xiaofeng Zhou, Jiarui Wang, Jonathan Herrmann, W. E. Moerner, Lucy Shapiro

Correspondence: Lucy Shapiro
Email: shapiro@stanford.edu

This PDF file includes:

Supplementary information
Figs. S1 to S11
Tables S1
References for SI citations

www.pnas.org/cgi/doi/10.1073/pnas.1906119116

Supplementary information

Supplementary results

Lon is constitutively active during Caulobacter cell cycle.

We generated an exogenous Lon substrate by tagging the C-terminus of the eYFP protein with a sul20C Lon degradation tag (1) driven by the P_{xyl} promoter with its constitutive expression induced by xylose. We observed that eYFP-sul20C was degraded by Lon in a wild-type background, but not in the *lon* mutant (SI Appendix, Fig. S1A). The instability of eYFP-sul20C was also confirmed by measuring cellular fluorescence intensity (SI Appendix, Fig. S1B). The eYFP-sul20C substrate was used to assess Lon proteolytic activity in swarmer, stalked, and pre-divisional cells obtained from synchronized cultures. The results demonstrate that the degradation rate of eYFP-sul20C is not significantly different in three types of cells, suggesting that Lon activity is cell cycle-independent (SI Appendix, Fig. S1C). We posit that cell-type specific CcrM proteolysis is likely due to the involvement of other accessory factors *in vivo*.

Caulobacter Lon binds chromosomal DNA in vivo

To test if *Caulobacter* Lon binds chromosomal DNA in vivo, an integrating plasmid bearing a translational fusion of eYFP to the C-terminus of Lon under the control of P_{xyl} was introduced into the chromosome of a temperature-sensitive (*ts*) mutant that forms filamentous cells when grown at the restrictive temperature, generating large DNA-free regions (2). A similar construct was made using a Lon DNA-binding deficient mutant LonQM (K301E/K303E/K305E/K306E) (SI Appendix, Fig. S7C) based on a recent study (3). Cultures of the *ts* mutant bearing the Lon-eYFP construct were grown at restrictive temperature in the presence of xylose and imaged by epifluorescence microscopy. We observed that Lon-eYFP co-localized with the DAPI DNA signal and was absent in DNA-free regions (SI Appendix, Fig. S2). In contrast, the LonQM-eYFP signal was observed throughout the entire cell, including the DNA-free regions (SI Appendix, Fig. S2).

Co-immunoprecipitation (Co-IP) of CcrM-Lon-DNA nucleoprotein complexes

We first conducted Co-IP using low concentrations of CcrM substrate (0.4 μM). CcrM co-immunoprecipitated with LonS674A only if DNA was present, demonstrating that DNA facilitates the recognition of CcrM by Lon (SI Appendix, Fig. S4C). Only a small fraction of CcrM co-immunoprecipitated with LonS674A in the absence of DNA under the physiological concentrations (1 μM) of CcrM (SI Appendix, Fig. S4C). When we performed similar assays using elevated concentrations of the CcrM substrate (4 μM), CcrM co-immunoprecipitated with LonS674A, independent of the presence of DNA (SI Appendix, Fig. S4C).

C-terminal domain of CcrM is required for its DNA binding activity and Lon recognition

Truncations lacking the N-terminal 294 residues of CcrM (CcrM65C) or the C-terminal 65 amino acids (CcrMΔC65) were generated and fused to eYFP (SI Appendix, Fig. S5B). *In vivo* degradation assays revealed that eYFP-CcrM65C was extremely unstable in the presence of Lon, with a half-life of ~ 3 min, whereas eYFP-CcrMΔC65 was stable (SI Appendix, Fig. S5B). In the absence of Lon, both eYFP-CcrM65C and eYFP-CcrMΔC65 were stable (SI Appendix, Fig. S5B), indicating that CcrM C-terminus is required for Lon recognition. To determine the precise amino acid sequence of the CcrM degradation tag within the C-terminal 65 amino acids, we generated a series of truncations based on the eYFP-CcrM65C construct (SI Appendix, Fig. S5B). Turnover of the chimeric proteins was quantified using a fluorescent microplate reader. The fluorescence levels of wild-type *Caulobacter* strains harboring plasmids expressing eYFP chimeric protein containing 24, 26, 28, 30, or 65 amino acids were all significantly depressed, suggesting that the C-terminal 24 amino acids of CcrM are sufficient to confer Lon-dependent proteolysis (SI Appendix, Fig. S5C).

Sequence alignment of the CcrM C-terminus revealed four highly conserved motifs among CcrM homologues in α-proteobacteria (SI Appendix, Fig. S6A). A conserved residue within each motif was mutated and each construct was introduced into a *ccrM* depletion strain and expressed under the control of the native *ccrM* promotor. CcrM bearing mutations at S315 and W332 caused severe cell cycle defects, including loss of viability and filamentous morphology (SI Appendix, Figs. S6B-S6D). *In vitro* gel shift assays showed that wild type CcrM binds Probe 1, but CcrMS315A does not, indicating that the S315 mutation abolished DNA binding activity (Fig. 5E).

Supplementary methods

Caulobacter synchronization

The synchronization experiment was performed as previously described (4). The synchronized swarmer cells were released into M2G medium supplied with certain antibiotics as needed. Samples were taken every 20 min for further analysis as indicated in the figure. For the double-synchronization experiment, the swarmer cells raised from the first synchronization were released and grown into M2G medium at 30 °C. Cells were collected at 160 min post-synchrony (mps) and subjected to the second synchronization. The swarmer and stalked fractions were collected, released into M2G, and monitored for cell cycle progression every 20 min.

Protein purification

Caulobacter Lon and its variants were purified using a combination of Ni-NTA affinity and size exclusion chromatography steps. ER2566 (NEB) harboring pET28b-Lon plasmid was grown in LB containing 50 µg/ml kanamycin and 3% ethanol, and protein expression was induced overnight at 16 °C with 1 mM IPTG at OD_{600} of 0.5. Cells were harvested and resuspended in purification buffer (50 mM HEPES pH 7.5, 100 mM NaCl, 100 mM KCl, 25mM imidazole, 10% Glycerol). After sonication, buffer-equilibrated Ni-NTA beads were added to cleared cell lysate, incubated at 4 ºC for 1 hour, and washed extensively with purification buffer. The target protein was eluted with purification buffer containing 325 mM imidazole. The protein sample was buffer exchanged to column buffer (50 mM HEPES pH 7.5, 100 mM NaCl, 100 mM KCl, 2 mM β-ME), loaded on a Sephacryl S-200 column. Fractions containing Lon were pooled, concentrated, dialyzed against protein storage buffer (50 mM HEPES pH 7.5, 100 mM NaCl, 100 mM KCl, 10% Glycerol), and stored at -80 ºC. CcrM and its variants were purified similarly to Lon. The removal of 6xHis tag was performed using Thrombin CleanCleave Kit (Sigma) and verified via immunoblot using anti-His antibody.

Microscale thermophoresis (MST)

Fluorescent labeling of lysine residues in LonS674A was accomplished by incubating each protein with an N-hydroxysuccinimide (NHS) ester conjugated to Atto-488 (Sigma-Aldrich). The dye-conjugate was dissolved in dry DMSO to make a 1 mM solution. The conjugation reaction was performed in the dark using 1-2 mg/mL protein and a 3-fold molar ratio of dye to protein at room temperature, with gentle shaking. Unconjugated dye was removed through dialysis against the protein storage buffer. Direct binding between fluorescently labeled LonS674A and CcrM or Probe 1 was probed via microscale thermophoresis (NanoTemper Technologies) (5). For each binding experiment, a twofold serial dilution was made for CcrM or Probe 1 in protein storage buffer with 0.025% Tween-20 and 10 mM $MgCl_2$. Fluorescently labeled LonS674A was then added at 25 nM, mixed, and incubated at room temperature for 10 minutes, covered, in the dark. The protein mixtures were loaded into Standard Treated capillaries (NanoTemper). Binding was assessed using the following instrument settings: 70% blue LED power, 40% IR-laser power, 30 second IR heating period, 5 second recovery.

Binding data were initially fit in MO.Affinity Analysis (NanoTemper), and the binding curve plateau data were exported. Experimental replicates were averaged in Prism 7 (GraphPad) and according to the law of mass action, as described:

$$\frac{BL}{B_0} = \frac{([L_0] + [B_0] + K_d) - \sqrt{(([L_0] + [B_0] + K_d)^2 - 4 * [L_0] * [B_0])}}{2[B_0]}$$

In this equation, BL represents the concentration of protein complexes, [B_0] represents total binding sites of the fluorescent ligand, [L_0] represents the amount of added ligand, and K_d represents the dissociation constant.

Protein in vivo and in vitro degradation assays

For protein *in vivo* degradation assay, cells were grown under the desired conditions. Protein synthesis was blocked by addition of 200 μg/ml chloramphenicol and 1 mg/ml spectinomycin. Samples were taken at the time-points indicated in the figure and snap-frozen in liquid nitrogen before immunoblot analysis. The relative protein remaining was calculated based on quantification of blot band intensity using ImageJ. Two biological replicates were performed, and each replicate was quantified with two different exposure times.

In vitro degradation assays were performed in Lon degradation buffer (100 mM KCl, 10 mM $MgCl_2$, 1 mM DTT, and 25 mM Tris-HCl [pH 8.0]) at 30 °C with an ATP-regeneration system (10 U/ml rabbit muscle pyruvate kinase [or 75 μg/ml creatine kinase], 20 mM phosphoenolpyruvate [or 20 mM creatine phosphate], 4 mM ATP). The concentrations of protease and substrate are indicated in the figure legend. Samples were taken every 30 min, quenched with SDS loading buffer, heated at 95 °C, and snap-frozen in liquid nitrogen. Samples were pre-warmed at 65 °C prior to separation by SDS-PAGE. The gels were stained by Coomassie blue G-250. Protein degradation rates were calculated based on quantification of protein band intensity using ImageJ.

CcrM remaining levels during the reaction time were fit to a single exponential model equation

$$Y = A_0 \times e^{-k \times X} + B$$

where Y is CcrM protein remaining, X is reaction time (min.), A0 is the initial amount of substrate (normalized to 1), *k* is degradation rate, and B is the fitting background. The fitting parameters over DNA concentrations were listed as follows:

DNA concentration (nM)	k (min^{-1} Lon_6^{-1})
0	0.0053 ± 0.0008
0.625	0.0054 ± 0.0008
1.25	0.0079 ± 0.0009
2.5	0.0138 ± 0.0012
5	0.0149 ± 0.0014

10	0.0197 ± 0.0027
20	0.0270 ± 0.0015
40	0.0227 ± 0.0025

In Fig. 3B, CcrM degradation rates over DNA concentrations were fit to an agonist-stimulated dose-response model (Prism 7):

$$CcrM\ degradation\ rate = V_{min} + \frac{(V_{max} - V_{min}) \times [DNA]}{K_{activation} + [DNA]}$$

with fitted parameters: V_{min} = 0.0039 ± 0.0016, V_{max} = 0.0289 ± 0.0022 min^{-1} Lon_6^{-1}, $K_{activation}$ = 4.391 ± 1.609 nM for DNA stimulation.

Quantitative reverse transcription PCR

Cells grown under the desired conditions were harvested, treated with two volumes of RNAprotect Bacteria Reagent (Qiagen), and snap-frozen in liquid nitrogen. The total RNA was extracted using the Qiagen RNeasy Mini Kit. Contaminated genomic DNA was removed through on-column digestion with a DNase using the Qiagen RNase-free DNase Kit. The RNA concentration was determined using a NanoDrop 2000 spectrophotometer (Thermo Scientific). Reverse transcription and cDNA synthesis were performed using QuantiTect Reverse Transcription Kit. Quantitative PCRs were performed using Luna Universal qPCR Master Mix (NEB) on an Applied Biosystems 7500 Fast Real-Time PCR system. The *rho* gene was used as an endogenous control. The relative fold change in target gene expression was calculated using a $2^{-\Delta\Delta C_T}$ method (6).

Measurement of fluorescence intensity in living cells

Cells grown under the desired condition were diluted to OD_{600} of 1. A 300 µl aliquot of cell suspension was added to the each well of a 96-well plate. The absolute fluorescence intensity was measured using Tecan Infinite M1000 plate reader at the High-Throughput Bioscience Center (HTBC), Stanford.

In vitro DNA methylation and ATPase assays

Probe 1 was amplified from NA1000 genome using primer pair probe1-F/probe1-R. Probe 2 was generated by double-joint PCR, using Probe 1 as a template. Two resultant fragments amplified by primer pairs probe1-F/probe1-RMu and probe1-FMu/probe1-R were jointed using the second-round of PCR with primer pair probe1-F/probe1-R. Probe 3 was amplified from NA1000 genome using primer pair probe3-F2/probe3-R2. To prepare fully methylated DNA probe, 20 nM Probe 1 was incubated with 420 nM CcrM and 80 µM S-adenosyl-methionine (SAM) at 30 °C for 1 hour in DNA methylation buffer (50 mM Tris-HCl [pH 7.5], 5 mM β-ME, 10 mM EDTA). The

resultant DNA probe was precipitated with 100% ethanol, washed twice with 70% ethanol, dried in speed-vac, and re-dissolved in distilled-water. To prepare hemi-methylated Probe 1, an equal amount of fully methylated and unmethylated Probe 1 was mixed in a PCR tube. The denature and annealing were performed on a thermocycler with 3 min at 95 ºC following 3 min at 70 ºC for 5 cycles. The resultant DNA probe was precipitated with 100% ethanol, dried in speed-vac, and re-dissolved in distilled-water. The methylation state of probe was assayed by restriction digestion using *Hin*fI or *Hph*I. Lon ATPase activity was assayed using ATPase/GTPase Activity Assay Kit (Sigma).

Single-molecule localization microscopy

Two color 2D single-molecule localizations were acquired on a home-built epifluorescence microscope as described (7). *Caulobacter* strains XZC260 and XZC294 were cultured to log phase in M2G. Cells that contain proteins labeled with eYFP and PAmCherry1 were detected on an inverted fluorescence microscope using an sequential pulse sequence of 405 nm (Coherent Obis, 0.1 W/cm^2: PAmCherry1 activation), 514 nm (MPB 2RU-VFL-1000-514 fiber laser, 1 kW/cm^2: eYFP blinking and detection), and 561 nm (Coherent Sapphire 561–100 CW, 0.8 kW/cm^2: PAmCherry1 detection) illumination. Reported laser intensity was measured at the stage with a Newport power meter (model 1918-C) and estimating the FWHM spot size by fitting the average autofluorescence from a plain agarose sample to a 2D Gaussian using custom MATLAB script. We used 50 ms integration time for all data acquisition. Fluorescence was split into two color channels and imaged on different parts of the EMCCD camera chip. Sample drift was compensated by localizing fluorescent beads (540/560 FluoSpheres, ThermoFisher) spin coated to the coverslip. High frequency noise in the drift was removed using moving average filtering in MATLAB (8). Background was subtracted by a pixel-by-pixel temporal median filter using a custom MATLAB program. We used ThunderSTORM (ImageJ) for localization analysis of single Lon-eYFP and PAmCherry-PopZ, as well as diffraction-limited CcrM-eYFP clusters. The analysis filter was the default wavelet filter B-spline. A connectivity of 8 and a threshold of 2 times the standard deviation of the high pass filter from the wavelet ((2*std(Wave.F1)) were used for particle detection. The particle locations were then determined by fitting the point spread function to an elliptical Gaussian using a weighted least squares method.

Localization precision was estimated by taking the standard deviation of positions of immobile molecules that were on in multiple frames. Single molecule localization images included in this paper, have an average localization precision of 22.4 nm in x and y for PAmCherry and 21.6 nm in x and y for eYFP. The localizations of PAmCherry-PopZ molecules that were on for multiple frames were averaged and reported as one localization, while all Lon-eYFP localizations were

reported. The PAmCherry-PopZ localizations were then transformed onto the image with Lon-eYFP localizations using a transformation function calculated as described (8) A locally weighted transformation function to register the two-color data was generated by imaging ~3000 fluorescent beads (FluoSpheres Carboxylate-modified microspheres, ThermoFisher) emitting in both channels. Fiducial registration errors and target registration errors both ranged from 4 to 12 nm across the field of view.

Single-molecule localization image rendering and Pearson correlation analysis

The correlation between PAmCherry-PopZ and Lon-eYFP as well as PAmCherry-PopZ and eYFP-CcrM was determined using a custom MATLAB program. Cell ROIs were manually identified, and ones containing more than 250 localizations of Lon-eYFP and 50 single PopZ molecules at the poles were used for calculation. For the diffraction-limited CcrM data, the camera pixel brightnesses and locations were used. 2D histograms of PAmCherry-PopZ and Lon-eYFP localizations were generated using a bin size of 25 nm. The Pearson Coefficient between the two color data was analyzed using the function $rho(a,b) = \frac{\sum_{i=1}^{n}(X_{a,i}-\bar{\bar{X}}_a)\,(Y_{b,i}-\bar{\bar{Y}}_b)}{\{\sum_{i=1}^{n}(X_{a,i}-\bar{\bar{X}}_a)^2 \sum_{j=1}^{n}(Y_{b,i}-\bar{\bar{Y}}_b)^2\}^{1/2}}$ where Xa and Yb are the number of localizations in each bin.

Supplementary Figure 1. In vivo stability of eYFP-sul20C.

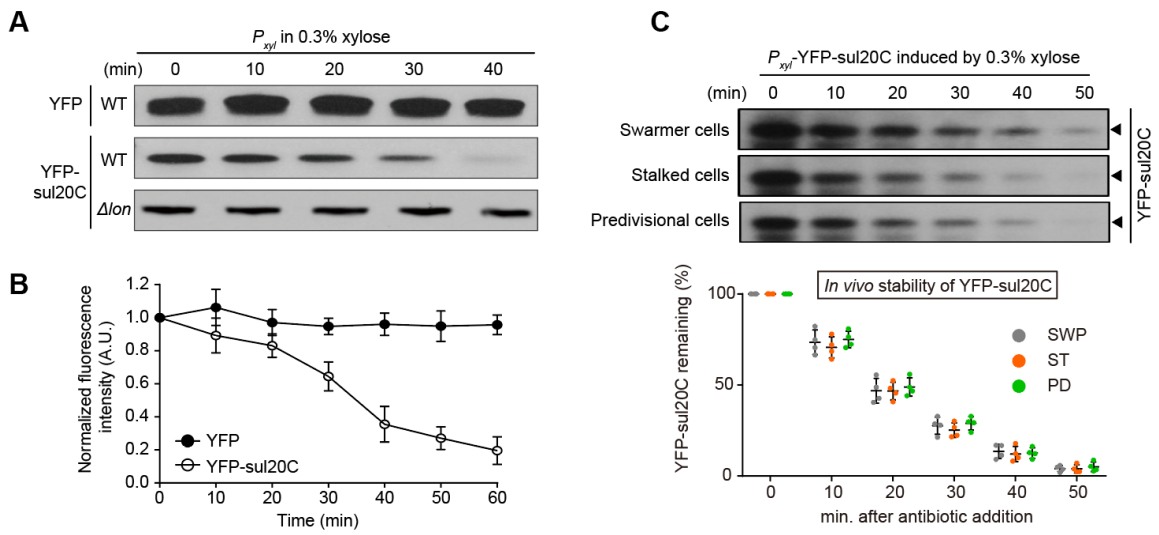

(A) *In vivo* degradation assays showing stability of either eYFP or eYFP-sul20C in wild-type cells. eYFP-sul20C stability in Δ*lon* cells is shown for comparison. Cells expressing free eYFP or eYFP-sul20C were grown in PYE supplemented with 0.3% xylose to exponential phase and treated with chloramphenicol (200 µg/ml) to shut-off protein synthesis. Protein levels were monitored by immunoblots using anti-GFP antibody.

(B) A graph of normalized cellular florescent intensity of eYFP or eYFP-sul20C is shown. The means ± SDs (n = 4) are plotted.

(C) *In vivo* degradation assays showing eYFP-sul20C stabilities in the swarmer, stalked, and predivisional cells. Cells expressing eYFP-sul20C controlled by P_{xyl} were grown in M2G with 0.3% xylose, synchronized, and harvested at 0, 45, and 120 min post-synchrony (mps). Samples were treated chloramphenicol (200 µg/ml) to shut-off protein synthesis. Top: Protein levels were monitored by immunoblots using anti-GFP antibody. Bottom: Relative protein remaining was plotted, and error bars represent SDs (n = 4).

Supplementary Figure 2. Lon binds to chromosomal DNA in *Caulobacter*

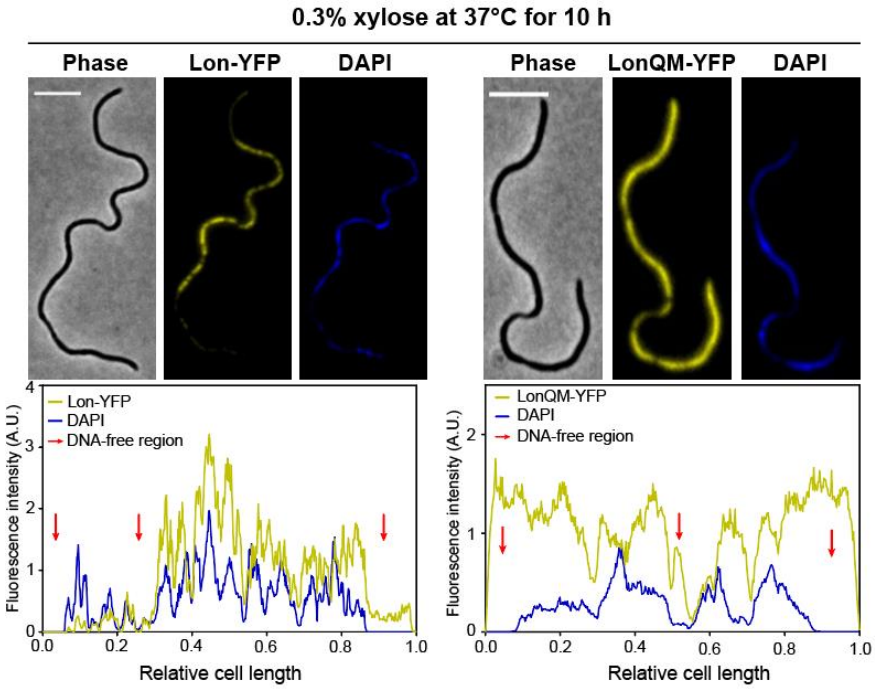

Fluorescence images showing Lon-eYFP colocalizing with DAPI-stained DNA in a *Caulobacter* temperature-sensitive *parE* and *ftsA* mutant (PC6340) that produces cell filamentous forms with DNA-free regions. LonQM-eYFP lacking DNA binding activity is shown for comparison. Cells were cultured at the restrictive temperature (37°C) for 10h in M2G medium with 0.3% xylose prior to DAPI staining and imaging (top). Scale bar = 5 μm. Fluorescence intensity profiles of Lon-eYFP or LonQM-eYFP and DAPI signals along the long axis of the cell are shown (bottom). Red arrows indicate DNA-free regions.

Supplementary Figure 3. Binding of CcrM or Lon to DNA is independent of DNA methylation sites

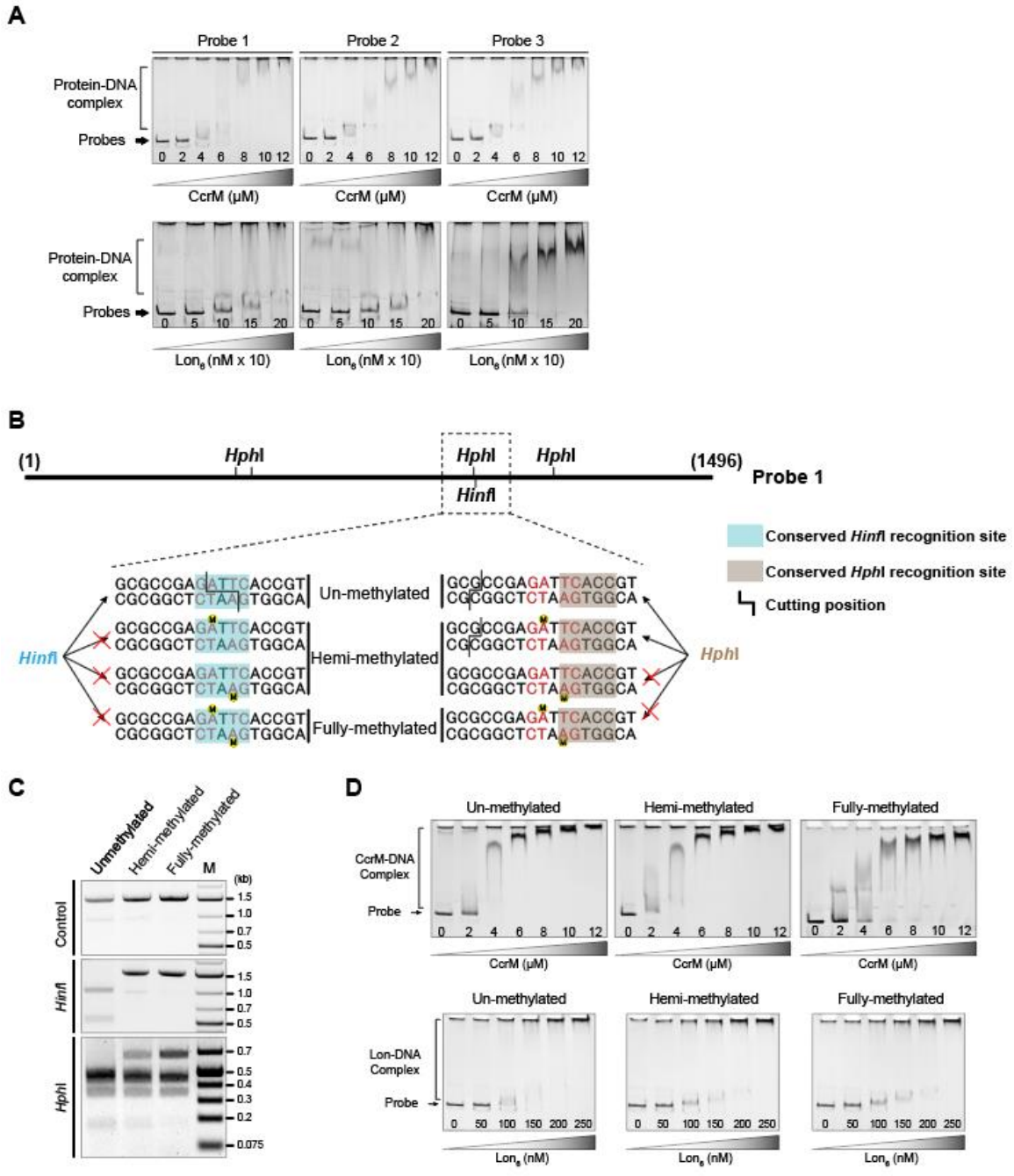

(A) Electrophoretic mobility shift assay showing binding of purified CcrM, or Lon to Probe 1, 2, and 3 (described in Fig. 2), respectively.

(B) Schematic view of restriction sites on Probe 1 and rationale of restriction digest-based DNA methylation assay. *Hinf*I is only able to cut unmethylated GANTC site (blue). *Hph*I cuts GGTGA$(N)_8$ that overlaps half of a GANTC site (brown). Adenine methylated GGTG$A_m(N)_8$ is resistant to *Hph*I digestion.

(C) Agarose gels showing the verification of DNA methylation states by restriction digest with *Hinf*I and *Hph*I. Two DNA fragments are expected for *Hinf*I digestion.

(D) Electrophoretic mobility shift assays showing CcrM and Lon binding to unmethylated, hemi-methylated and fully-methylated Probe 1, respectively.

Supplementary Figure 4. DNA facilities CcrM recognition by Lon under the physiological conditions

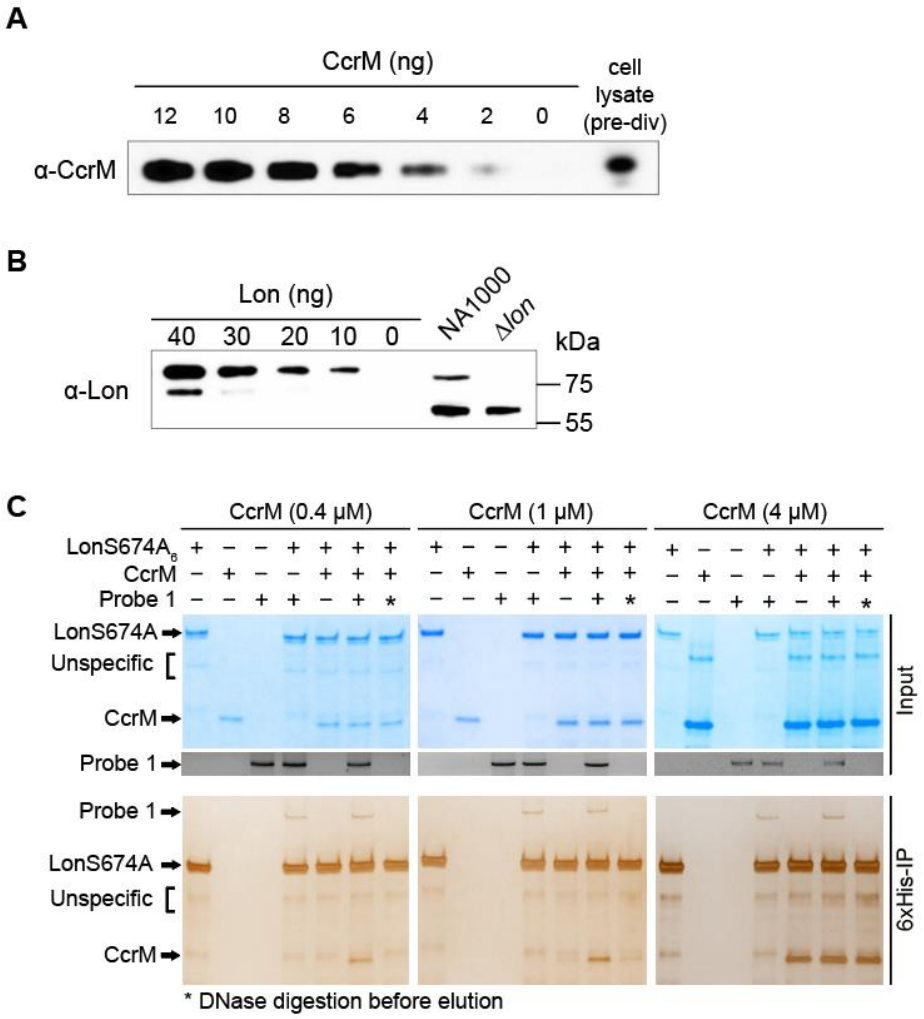

(A) Quantitative immunoblots of CcrM levels in *Caulobacter* pre-divisional cells. Immunoblots were performed following SDS-PAGE of different concentrations of purified CcrM and a *Caulobacter* pre-divisional cell lysate collected at 120 mps. The intracellular concentration of CcrM was 1090 ± 135 nM or ~ 600 ± 150 CcrM monomers per cell.

(B) Quantitative immunoblots of Lon levels in *Caulobacter* pre-divisional cell. Immunoblots were performed following SDS-PAGE of different concentrations of purified Lon and a *Caulobacter* pre-divisional cell lysate collected at 120 mps. The *lon*

deletion mutant serves as a negative control to distinguish unspecific bands. The intracellular concentration of Lon was 2480 ± 325 nM or ~ 1490 ± 200 Lon hexamers per cell.

(C) DNA facilitates recognition of low concentrations of CcrM by LonS674A. Silver-stained SDS-PAGE gels showing co-immunoprecipitation of nucleoprotein complex. The concentration of $LonS674A_6$ was maintained at 0.2 µM. A low concentration of CcrM (0.4 µM) requires the presence of DNA to be recognized by LonS674A, whereas the recognition of a high concentration of CcrM (4 µM), which is ~ 4-fold higher than CcrM concentration in the cell (950 - 1280 nM), does not depend on the presence of DNA. Asterisks indicate DNase I digestion before elution.

Supplementary Figure 5. C-terminal 65 amino acid of CcrM is required for its DNA binding activity and the final 24 amino acids is required for Lon recognition

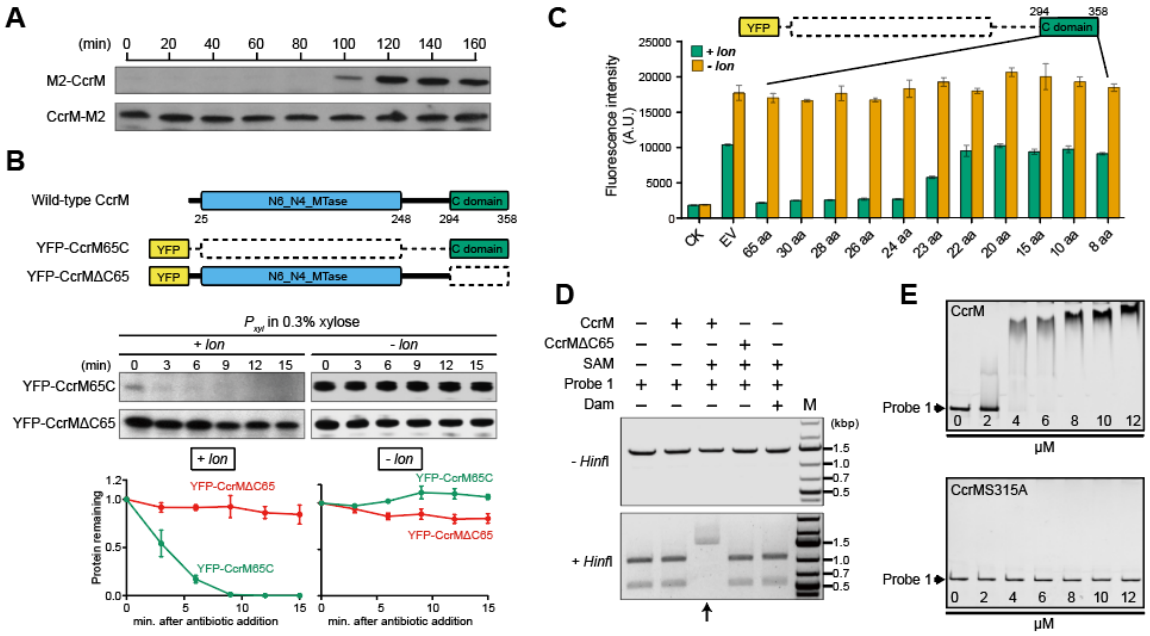

(A) Cells containing a single copy of M2-CcrM or CcrM-M2 under the control of native promotor were grown in M2G, synchronized, and released onto fresh M2G. Samples were taken every 20 min for immunoblots with anti-CcrM antibody.

(B) *In vivo* degradation assays showing the effect of C-terminal 65 residues on CcrM protein stability. CcrM domain structure and eYFP chimeric constructs used in this study are shown. Dash line indicates a deletion of amino acids. The numbers refer to amino acid positions. Stabilities of eYFP chimeric proteins in a *lon* mutant (- *lon*) are shown for comparison. Cells were grown in PYE with 0.3% xylose to exponential phase and treated with chloramphenicol (200 μg/ml) to inhibit protein synthesis. Protein levels were monitored by immunoblots using anti-GFP antibody (top). Band intensities were quantified (bottom) and error bars represent SDs (n = 4).

(C) Florescence of wild-type (+ *lon*) and a *lon* deletion mutant (- *lon*) harboring plasmids expressing variant CcrM proteins tagged with eYFP. A schematic shows a series of truncations in which 8, 10, 15, 20, 22, 23, 24, 26, 28, and 30 amino acids are retained from the CcrM C-terminal 65 amino acids. Fluorescence normalized by optical density is

represented by a bar graph. shown. The means ± SDs (n = 6) are plotted. CK, cells harboring no plasmid. EV, cells harboring empty vector expressing free eYFP.

(D) DNA methylation assays showing the effect of CcrM C-terminal domain on its DNA methyltransferase activity. PCR amplified Probe 1 was incubated with CcrM or CcrMΔC65 in the presence of S-adenosyl methionine (SAM). DNA methylation states were assayed by *Hin*fI digestion. *Hin*fI was unable to digest Probe 1 incubated with CcrM, indicating that the GATTC site was methylated. In contrast, Probe 1 incubated with CcrMΔC65 was digested by *Hin*fI, giving two fragments at 1.0 kb and 0.5 kb in length on agarose gels. Dam methylase from *E. coli* served as a negative control.

(E) Electrophoretic mobility shift assay showing abolished DNA binding activity caused by mutation at S315A on CcrM.

Supplementary Figure 6. Conserved Motif B and Motif C within CcrM C-terminal region are required for DNA methyltransferase activity

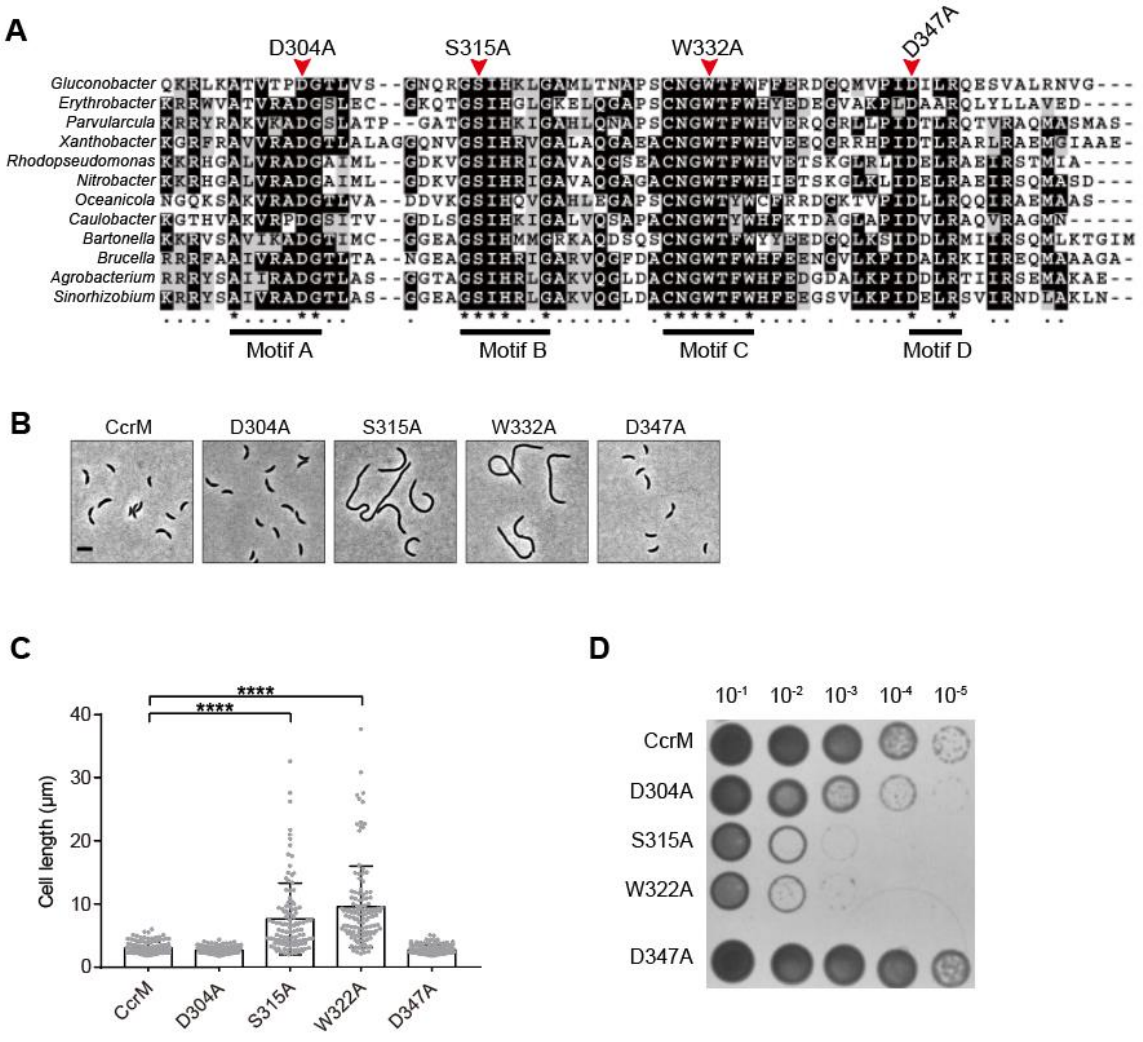

(A) Sequence alignment of CcrM homologs from twelve divergent α-proteobacterial species reveals four conserved motifs within 65 C-terminal amino acids. The conserved residues subjected to amino acid substitution in each motif are highlighted.

(B) Phase contrast micrographs of *ccrM* depletion strains complemented with CcrM, CcrMD304A, CcrMS315A, CcrMW332A or CcrMD347A. Scale bar = 5 µm.

(C) Cell length analyses of strains shown in (B). Mean cell length (µm) ± SEM: CcrM = 3.10 ± 0.08 (*n* = 128); CcrMD304A = 2.71 ± 0.05 (*n* = 120); CcrMS315A = 7.66 ± 0.54

(n = 112); CcrMW332A = 9.57 ± 0.59 (n = 120); CcrMD347A = 2.78 ± 0.06 (n = 133). **** indicates $P < 0.0001$ by one-way ANOVA.

(D) Spot dilutions of strains shown in (B). Cells in exponential phase were diluted to an OD600 of 0.03, serially diluted and spotted onto the same PYE agar plate and incubated at 30 °C for 2 days.

Supplementary Figure 7. DNA binding activities of CcrM and Lon mutants

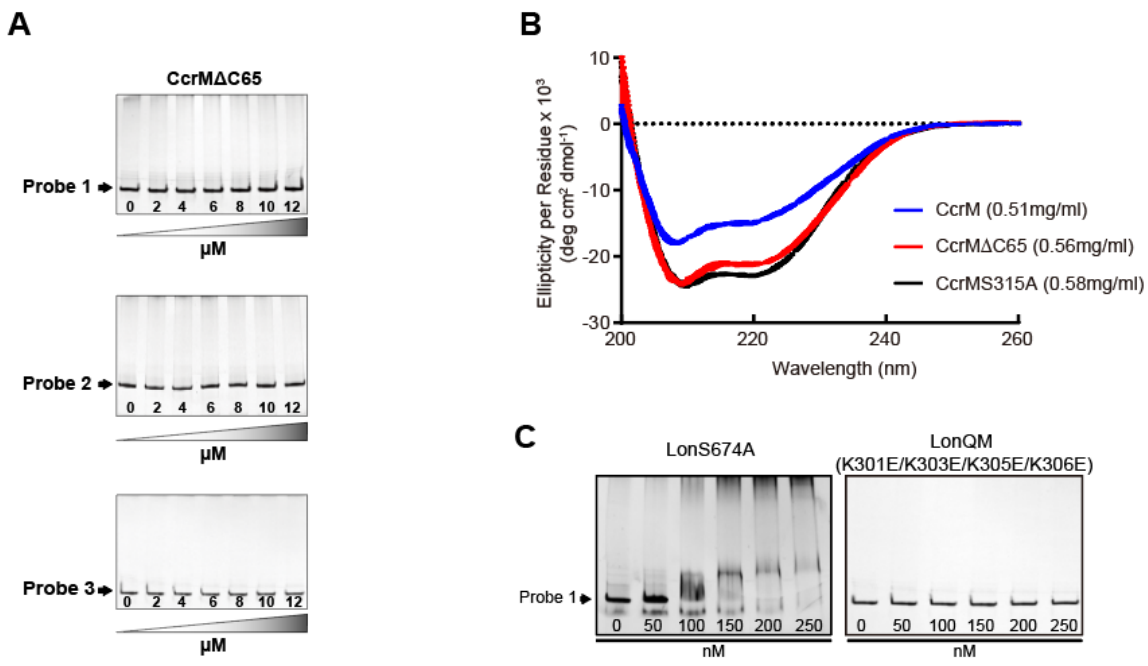

(A) Electrophoretic mobility shift assays showing that CcrM with a C-terminal deletion of 65 amino acids (CcrMΔC65) abolished DNA-binding to probes1,2 and 3 diagrammed in Fig. 2A.

(B) Circular dichroism spectra of CcrM (*blue*), CcrMΔC65 (*red*), and CcrMS315A (*black*). Protein concentrations are indicated. Each spectrum is an average of three scans, with standard error measurements shown.

(C) Electrophoretic mobility shift assay showing the effects of CcrM alanine substitution at S674 and glutamic acid substitutions at K301/K303/K305/K306 on Lon DNA binding activities.

Supplementary Figure 8. *In vitro* degradation assays related to Fig. 3

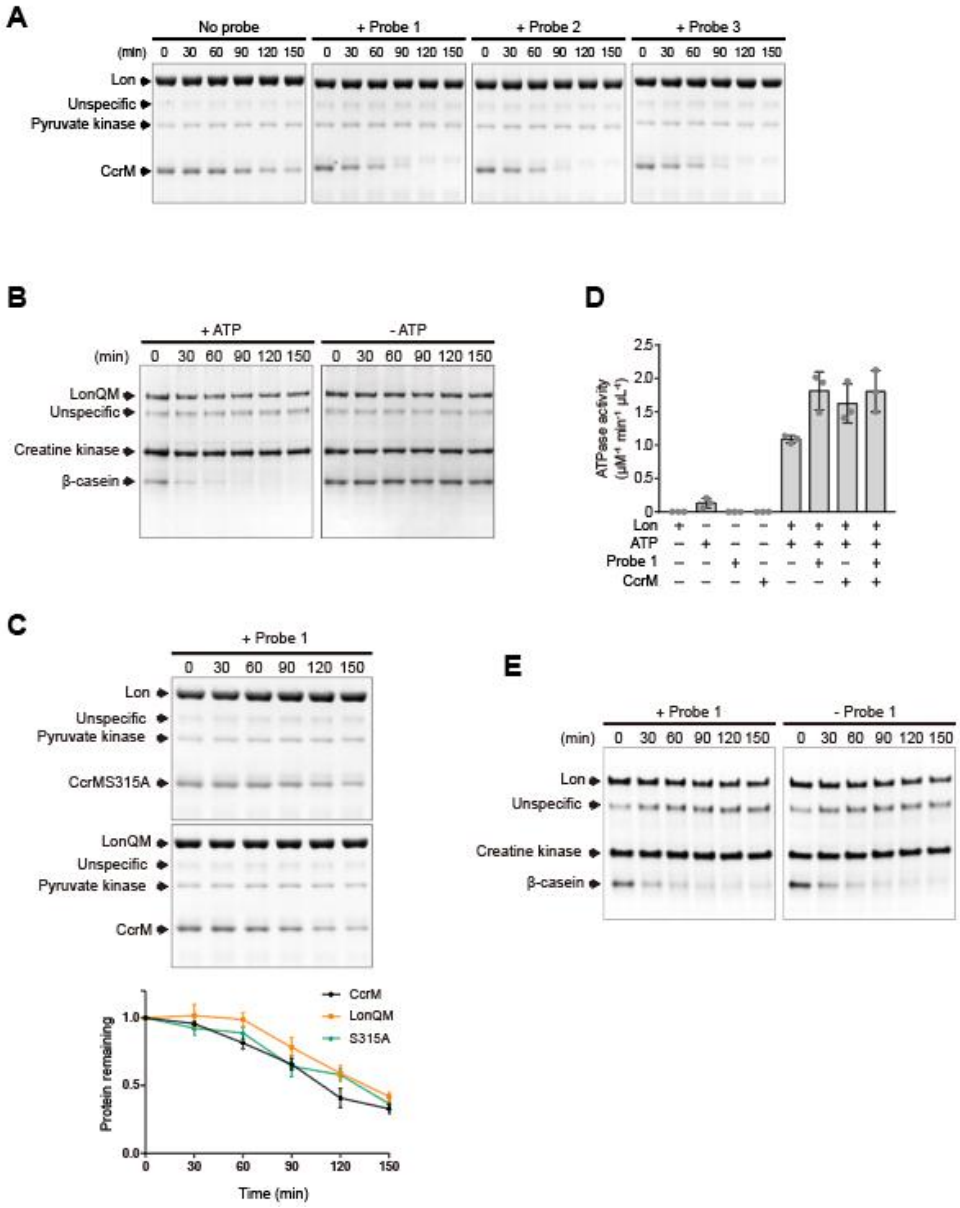

(A) *In vitro* degradation assays showing the stimulatory effect of DNA on CcrM degradation by Lon. CcrM (1 μM) was incubated with Lon_6 (0.25 μM) in the absence or presence of DNA probes (10 nM). Protein samples were collected every 30 min and analyzed by sodium dodecyl sulfate polyacrylamide gel electrophoresis.

(B) *In vitro* degradation assays showing the degradation of β-casein by LonQM. β-casein (1 μM) was incubated with $LonQM_6$ (0.2 μM) in the absence or presence of ATP (4 mM).

Protein samples were collected every 30 min and analyzed by sodium dodecyl sulfate polyacrylamide gel electrophoresis.

(C) *In vitro* degradation assays showing the degradation of CcrMS315A by Lon and the degradation of CcrM by LonQM. CcrMS315A or CcrM (1 μM) was incubated with Lon or $LonQM_6$ (0.25 μM) in the presence of Probe 1 (10 nM). Protein samples were collected every 30 min and analyzed by sodium dodecyl sulfate polyacrylamide gel electrophoresis. The intensity of CcrM band from three independent experiments was quantified. The means ± SDs (n = 3) are plotted.

(D) ATPase activity of Lon in the presence and absence of DNA and CcrM.

(E) *In vitro* degradation assays showing the degradation of β-casein by Lon in the presence and absence of DNA. β-casein (1 μM) was incubated with Lon_6 (0.2 μM) in the absence or presence of Probe 1 (10 nM). Protein samples were collected every 30 min and analyzed by sodium dodecyl sulfate polyacrylamide gel electrophoresis.

Supplementary Figure 9. Dynamic sequestration of CcrM in *Caulobacter*, related to Fig. 4

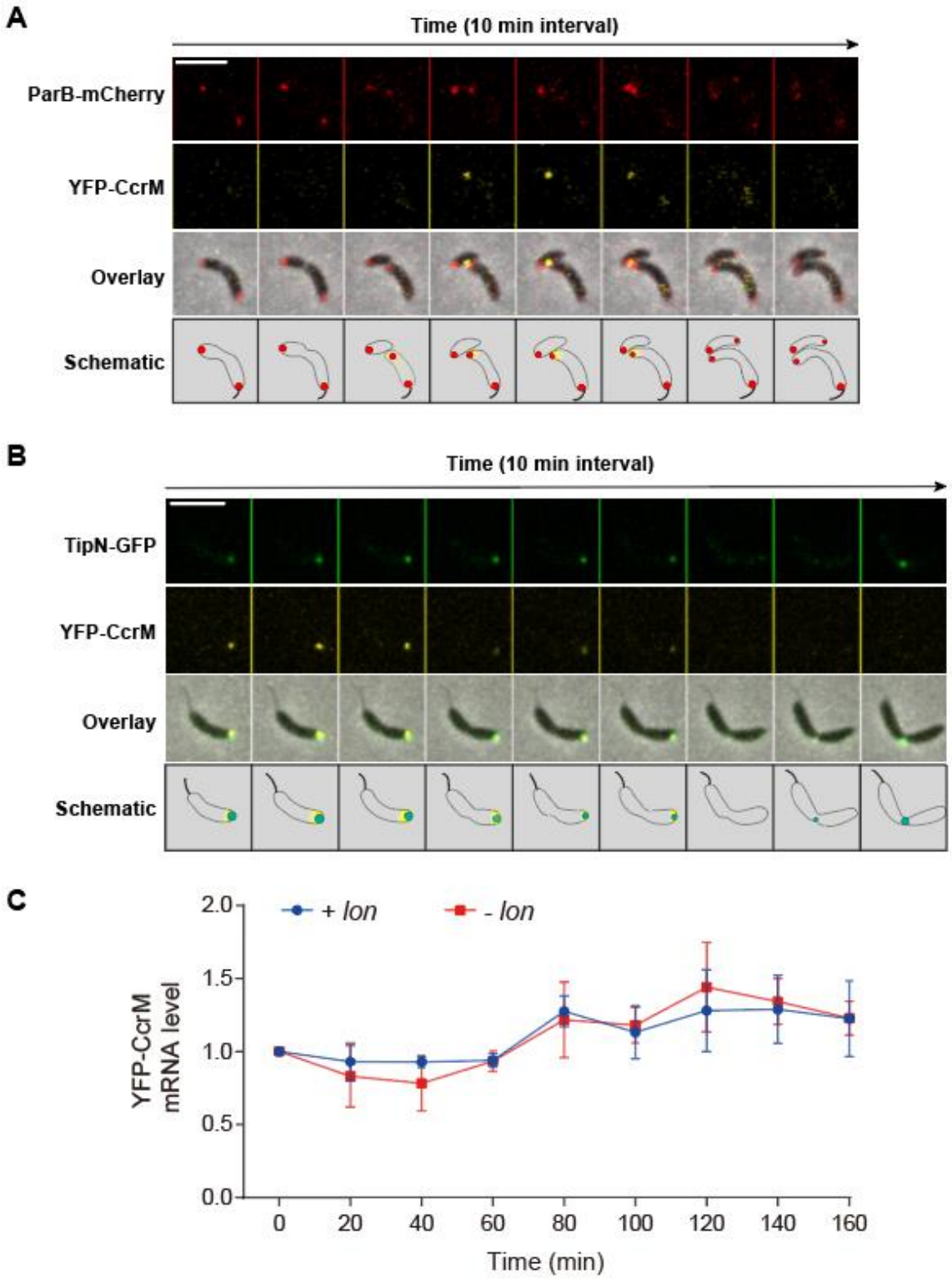

(A) Time-lapse microscopy of cells co-expressing chromosome-encoded eYFP-CcrM and the ParB-mCherry DNA partitioning protein under the control of their native promotors. eYFP-CcrM co-appeared with the ParB-*parS* complex at the new pole of the progeny stalked cell. Images of the cells were taken every 10 min. Scale bar = 5 μm.

(B) Time-lapse microscopy of cells co-expressing chromosome-encoded eYFP-CcrM and the TipN-GFP new cell pole marker under the control of their native promotors. eYFP-CcrM are released from the pole prior to the formation of the division plane. Images of the cells were taken every 10 min. Scale bar = 5 μm.

(C)eYFP-CcrM mRNA levels from each sample shown in Fig. 4E were normalized by qRT-PCR. The means ± SDs (n = 3) are plotted.

Supplementary Figure 10. Quantifications of cell length and CcrM polar localization in strains harboring single copy or multi-copies of e*yfp-ccrM* under the control of P_{xyl}

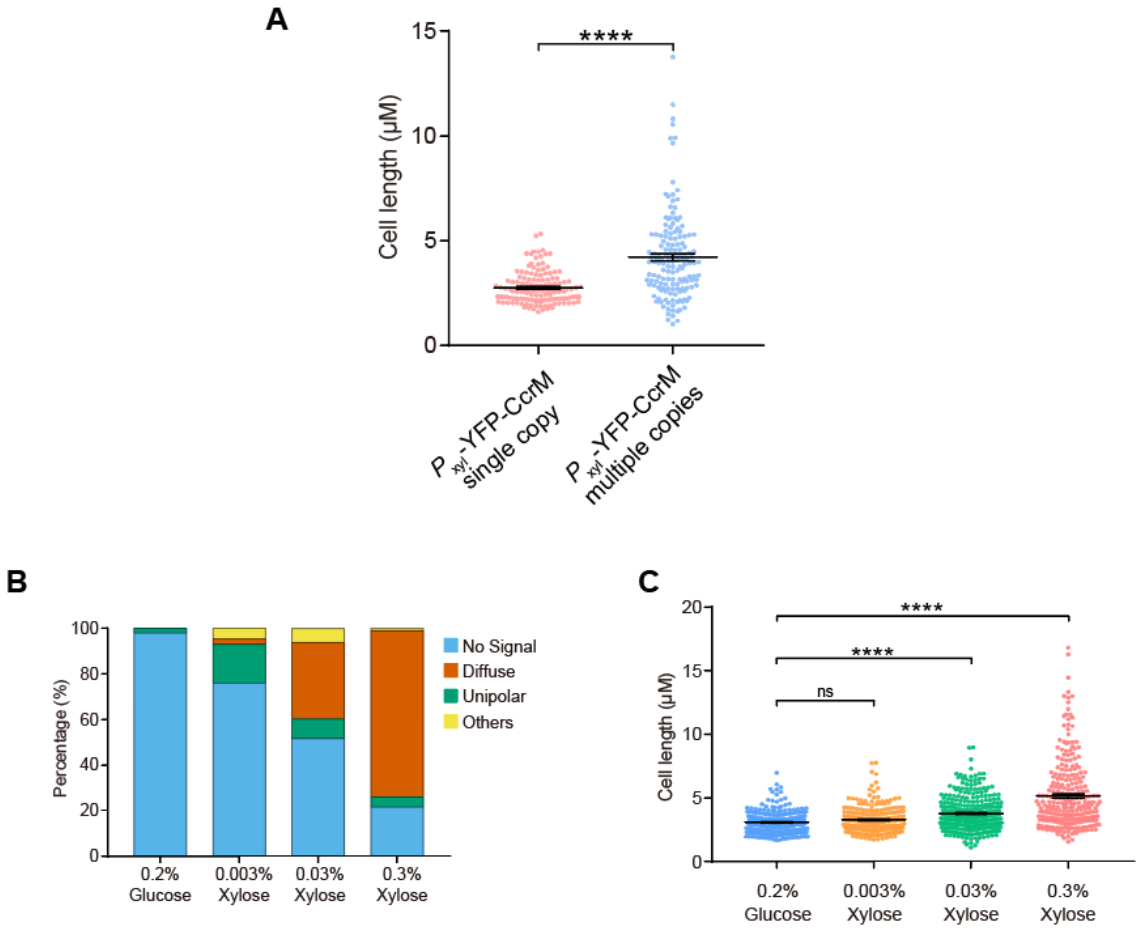

(A) Cell length analyses of strains in Fig. 6A. Mean cell length (μm) ± SEM: P_{xyl}-e*yfp-ccrM* single copy = 2.76 ± 0.07 (*n* = 137); P_{xyl}-e*yfp-ccrM* multi-copies = 4.21 ± 0.17 (*n* = 152). **** indicates *P* < 0.0001 by unpaired *t*-test.

(B) The percentage of cells harboring multi-copies of e*yfp-ccrM* classified by eYFP-CcrM localization in four different growth conditions.

(C) Cell length analyses under the four conditions described in (B). Mean cell length (μm) ± SEM: 0.2% Glucose = 3.08 ± 0.06 (*n* = 256); 0.003% xylose = 3.28 ± 0.07 (*n* = 234);

0.03% xylose = 3.78 ± 0.08 (n = 303); 0.3% xylose = 5.16 ± 0.17 (n = 270). **** indicates $P < 0.0001$ by one-way ANOVA. ns, not significant.

Supplementary Figure 11. Multiple polar localized proteins in *Caulobacter* are not required for CcrM polar sequestration

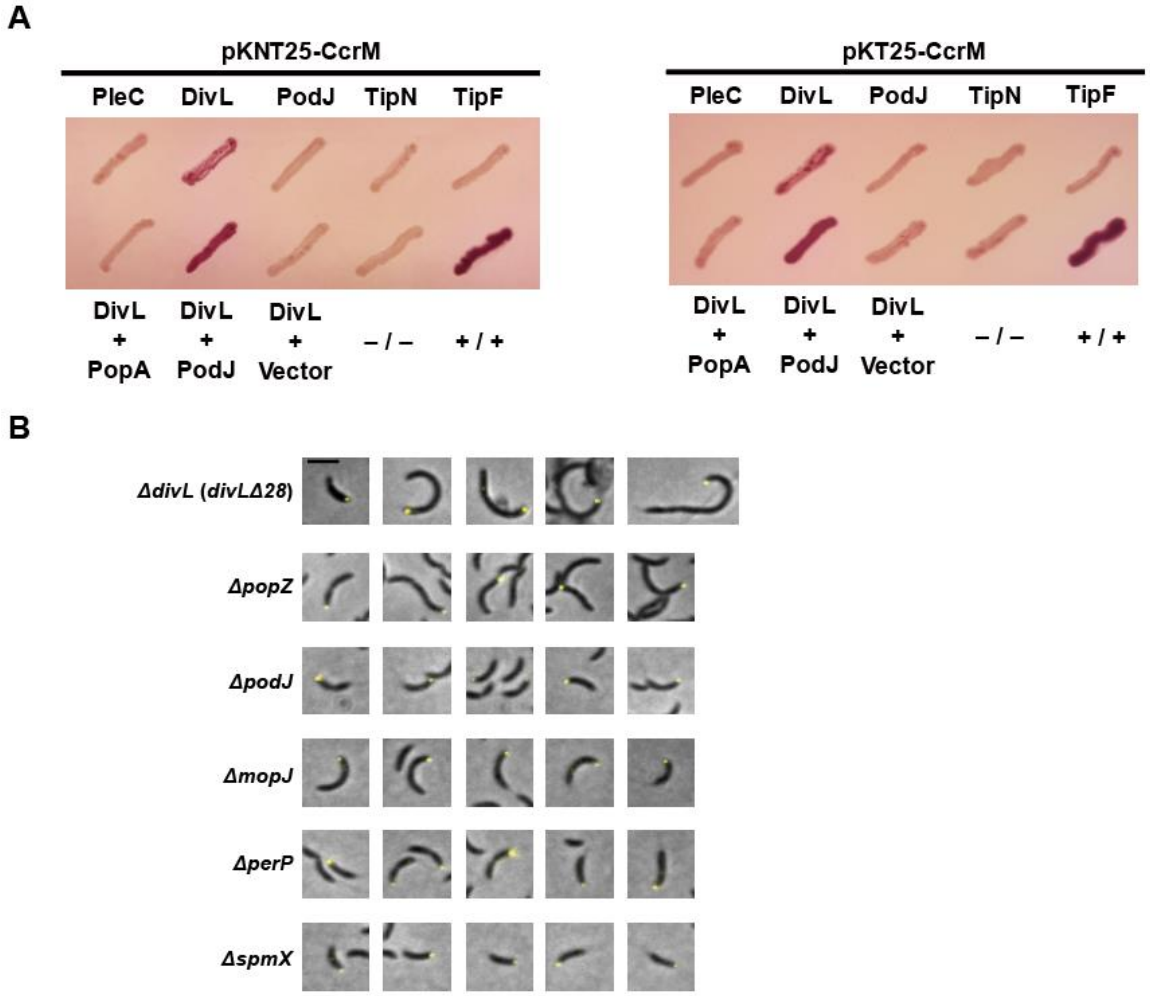

(A) Bacterial two-hybrid assays showing the negative interaction of CcrM to polar localized proteins (PleC, PodJ, TipN, and TipF). - / - and + / + indicate a negative and a positive control, respectively. Red colonies indicate a positive interaction. Cells were grown at 30 °C for 2 days before photography. DivL shows weak interaction with CcrM. However, CcrM polar localization still can be observed in *divL* mutant (see panel B). Thus, we consider this interaction as false positive or sticky interaction.

(B) Overlaid phase contrast and epifluorescence images showing CcrM polar sequestration in cells depleting several known new pole localized proteins and protease

regulator PerP. CcrM polar sequestration does not depend on the presence of DivL, PopZ, PodJ, MopJ, or PerP. Deletion of SpmX (localized to the old pole) serves as a negative control. Scale bar = 1 μm.

Table S1. Strains and plasmids used in this study.

Name	Description	Source
***E. coli* strains**		
NEB5alpha	General cloning strain	NEB
ER2566	BL21 derivative, *fhuA2 lacZ::T7 gene1 [lon] ompT gal sulA11 R(mcr-73::miniTn10--*Tet^S*)2 [dcm] R(zgb-210::Tn10--*Tet^S*) endA1 Δ(mcrC-mrr)114::IS10*	NEB
XZE55	ER2566, pET28b-CcrM	This study
XZE56	ER2566, pET28b-CcrMΔC65	This study
XZE195	ER2566, pET28b-CcrMS315A	
XZE58	ER2566, pET28b-Lon	This study
XZE156	ER2566, pET28b-LonS674A	This study
XZE207	ER2566, pET28b-LonQM	This study
BTH101	for bacterial two-hybrid. *F⁻, cya-99, araD139, galE15, galK16, rpsL1 (Str^r), hsdR2, mcrA1, mcrB1*	Lab collection
XZE89	BTH101, pKNT25, pUT18	This study
XZE90	BTH101, pKT25-Zip, pUT18C-Zip	Lab collection
XZE91	BTH101, pKNT25-CcrM, pUT18-PleC	This study
XZE92	BTH101, pKNT25-CcrM, pUT18-DivL	This study
XZE93	BTH101, pKNT25-CcrM, pUT18C-PodJ	This study
XZE94	BTH101, pKNT25-CcrM, pUT18-TipN	This study
XZE95	BTH101, pKNT25-CcrM, pUT18-TipF	This study
XZE96	BTH101, pKT25-CcrM, pUT18-PleC	This study
XZE97	BTH101, pKT25-CcrM, pUT18-DivL	This study
XZE98	BTH101, pKT25-CcrM, pUT18C-PodJ	This study
XZE99	BTH101, pKT25-CcrM, pUT18-TipN	This study
XZE100	BTH101, pKT25-CcrM, pUT18-TipF	This study
***C. crescentus* strains**		
LS101 (CB15N or NA1000)	Synchronizable derivative of wild-type CB15	Lab collection
LS2382	NA1000 *Δlon* (*spec^r*)	Lab collection
XZC13	NA1000 P_{ccrM}-*M2-ccrM*	This study
XZC14	NA1000 P_{ccrM}-*ccrM-M2*	This study
XZC34	NA1000, pXYFPN2-CcrM	This study
XZC35	NA1000, pXYFPN2-CcrM65C	This study
XZC36	NA1000, pXYFPN2-CcrMΔC65	This study
XZC154	*Δlon*, pXYFPN2-CcrM	This study
XZC161	*Δlon*, pXYFPN2-CcrM65C	This study
XZC88	*Δlon*, pXYFPN2-CcrMΔC65	This study
XZC5	NA1000, pXYFPN2	This study
XZC105	NA1000, pXYFPN2-CcrM30C	This study
XZC139	NA1000, pXYFPN2-CcrM28C	This study
XZC138	NA1000, pXYFPN2-CcrM26C	This study
XZC144	NA1000, pXYFPN2-CcrM24C	This study
XZC143	NA1000, pXYFPN2-CcrM23C	This study
XZC137	NA1000, pXYFPN2-CcrM22C	This study
XZC106	NA1000, pXYFPN2-CcrM20C	This study
XZC108	NA1000, pXYFPN2-CcrM15C	This study
XZC109	NA1000, pXYFPN2-CcrM10C	This study
XZC114	NA1000, pXYFPN2-CcrM8C	This study
XZC153	*Δlon*, pXYFPN2	This study
XZC160	*Δlon*, pXYFPN2-CcrM30C	This study
XZC159	*Δlon*, pXYFPN2-CcrM28C	This study
XZC158	*Δlon*, pXYFPN2-CcrM26C	This study
XZC162	*Δlon*, pXYFPN2-CcrM24C	This study
XZC163	*Δlon*, pXYFPN2-CcrM23C	This study
XZC157	*Δlon*, pXYFPN2-CcrM22C	This study
XZC164	*Δlon*, pXYFPN2-CcrM20C	This study
XZC156	*Δlon*, pXYFPN2-CcrM15C	This study
XZC155	*Δlon*, pXYFPN2-CcrM10C	This study
XZC165	*Δlon*, pXYFPN2-CcrM8C	This study
XZC6	NA1000, pXYFPN2-sul20C	This study
XZC86	*Δlon*, pXYFPN2-sul20C	This study
PC6340	Synthesizing temperature-sensitive forms of the cell division protein FtsA and the topoisomerase IV subunit ParE	Lab collection

XZC142	PC6340, pXYFPC2-Lon	This study
XZC148	PC6340, pXYFPC2-LonQM	This study
XZC24	NA1000 P_{ccrM}-*yfp-ccrM*	This study
XZC75	NA1000 P_{ccrM}-*yfp-ccrM*, pCHYC1-SpmX	This study
CJW1406	Expressing TipN-GFP under the control of P_{tipN}	(9)
XZC89	NA1000 P_{ccrM}-*yfp-ccrM*, P_{tipN}-*tipN-gfp*	This study
XZC112	NA1000 P_{ccrM}-*yfp-ccrM*, pCHYC1-ParB	This study
XZC121	NA1000 P_{ccrM}-*ccrMD304A*, P_{xyl}-*ccrM*	This study
XZC129	NA1000 P_{ccrM}-*ccrMD315A*, P_{xyl}-*ccrM*	This study
XZC135	NA1000 P_{ccrM}-*ccrMD322A*, P_{xyl}-*ccrM*	This study
XZC134	NA1000 P_{ccrM}-*ccrMD350A*, P_{xyl}-*ccrM*	This study
XZC131	NA1000 P_{ccrM}-*ccrMD347A*, P_{xyl}-*ccrM*	This study
XZC20	NA1000 P_{lon}-*lon-mCherry*	This study
XZC23	NA1000 P_{lon}-*mCherry-lon*	This study
JP463	P_{popZ}-PAmCherry-PopZ	Lab collection
XZC294	JP463, pYFPC2-LonC	This study
XZC260	XZC24, P_{popZ}-PAmCherry-PopZ	This study
XZC304	pMCS6-DnaAlocus-PdnaA-CYPF/pXYFPN2-CcrM	This study
XZC305	pMCS6-DnaAlocus-PctrA1-CYPF/pXYFPN2-CcrM	This study
XZC306	pMCS6-TrpElocus-PdnaA-CYPF/pXYFPN2-CcrM	This study
XZC307	pMCS6-TrpElocus-PctrA1-CYPF/pXYFPN2-CcrM	This study
XZC308	pMCS6-DnaAlocus-PdnaA-CYPF/pBXMCS2-YFP-CcrM	This study
XZC309	pMCS6-DnaAlocus-PctrA1-CYPF/pBXMCS2-YFP-CcrM	This study
XZC310	pMCS6-TrpElocus-PdnaA-CYPF/pBXMCS2-YFP-CcrM	This study
XZC311	pMCS6-TrpElocus-PctrA1-CYPF/pBXMCS2-YFP-CcrM	This study
LS4461	*ΔdivL(divLΔ28)*	(10)
XZC50	*ΔdivL(divLΔ28)* P_{ccrM}-*yfp-ccrM*	This study
GB255	*popZ::Ω*	(11)
XZC49	*ΔpopZ* P_{ccrM}-*yfp-ccrM*	This study
XZC68	*ΔpodJ* P_{ccrM}-*yfp-ccrM*	This study
XZC71	*ΔmopJ* P_{ccrM}-*yfp-ccrM*	This study
XZC69	*ΔperP* P_{ccrM}-*yfp-ccrM*	This study
XZC70	*ΔspmX* P_{ccrM}-*yfp-ccrM*	This study
Plasmids		
pNPTS138	integrating vector	Lab collection
pNP138-M2-CcrM	for generation of a markerless insertion of M2-CcrM	This study
pNP138-CcrM-M2	for generation of a markerless insertion of CcrM-M2	This study
pNP138-YFP-CcrM	for generation of a markerless insertion of YFP-CcrM	This study
pNP138-mCherry-Lon	for generation of a markerless insertion of mCherry-Lon	This study
pXYFPN2	integrating vector expressing N-terminal fusion of YFP under the control of P_{xyl}	(12)
pXYFPN2-CcrM	integrating vector expressing YFP-CcrM under the control of P_{xyl}	This study
pXYFPN2-CcrM65C	integrating vector expressing YFP-CcrM65C under the control of P_{xyl}	This study
pXYFPN2-CcrMΔC65	integrating vector expressing YFP- CcrMΔC65 under the control of P_{xyl}	This study
pXYFPN2-CcrM30C	integrating vector expressing YFP-CcrM30C under the control of P_{xyl}	This study
pXYFPN2-CcrM28C	integrating vector expressing YFP-CcrM28C under the control of P_{xyl}	This study
pXYFPN2-CcrM26C	integrating vector expressing YFP-CcrM26C under the control of P_{xyl}	This study
pXYFPN2-CcrM24C	integrating vector expressing YFP-CcrM24C under the control of P_{xyl}	This study
pXYFPN2-CcrM23C	integrating vector expressing YFP-CcrM23C under the control of P_{xyl}	This study
pXYFPN2-CcrM22C	integrating vector expressing YFP-CcrM22C under the control of P_{xyl}	This study
pXYFPN2-CcrM20C	integrating vector expressing YFP-CcrM20C under the control of P_{xyl}	This study
pXYFPN2-CcrM15C	integrating vector expressing YFP-CcrM15C under the control of P_{xyl}	This study
pXYFPN2-CcrM10C	integrating vector expressing YFP-CcrM10C under the control of P_{xyl}	This study
pXYFPN2-CcrM8C	integrating vector expressing YFP-CcrM8C under the control of P_{xyl}	This study
pXYFPN2-sul20C	integrating vector expressing YFP-sul20 under the control of P_{xyl}	This study
pET28b	expression vector for protein purification	Lab collection
pET28b-CcrM	expression vector for purification of CcrM	This study
pET28b-CcrMΔC65	expression vector for purification of CcrMΔC65	This study
pET28b-CcrM315A	expression vector for purification of CcrMS315A	This study
pET28b-Lon	expression vector for purification of Lon	This study
pET28b-LonS674A	expression vector for purification of LonS674A	This study
pET28b-LonQM	expression vector for purification of LonQM	This study
pXYFPC2-Lon	integrating vector expressing Lon-YFP under the control of P_{xyl}	This study
pXYFPC2-LonQM	integrating vector expressing LonQM-YFP under the control of P_{xyl}	This study
pMCS6-Plon-Lon	integrating vector expressing Lon under the control of P_{lon}	This study
pMCS6- Plon-LonQM	integrating vector expressing LonQM under the control of P_{lon}	This study

pXYFPN2-CcrMS315A	integrating vector expressing YFP-CcrMS315A under the control of P_{xyl}	This study
pYFPC2-LonC	integrating vector harboring $Lon_{508-799}$-YFP	
pCHYC1	integrating vector harboring C-terminal fusion of mCherry	(12)
pCHYC1-SpmX	integrating vector harboring $SpmX_{207-431}$-mCherry	This study
pCHYC1-ParB	integrating vector harboring $ParB_{104-304}$-mCherry	This study
pCHYC2-Lon	integrating vector harboring $Lon_{407-799}$-mCherry	This study
pXMCS2	integrating vector harboring a 153bp xylose-promotor	(12)
pXMCS2-CcrM	integrating vector harboring P_{xyl}-*ccrM*	This study
pXMCS2-CcrMD304A	integrating vector harboring P_{xyl}-*ccrMD304A*	This study
pXMCS2-CcrMS315A	integrating vector harboring P_{xyl}-*ccrMD315A*	This study
pXMCS2-CcrMW322A	integrating vector harboring P_{xyl}-*ccrMD322A*	This study
pXMCS2-CcrMR350A	integrating vector harboring P_{xyl}-*ccrMD350A*	This study
pXMCS2-CcrMD347A	integrating vector harboring P_{xyl}-ccrMD347A	This study
pBXMCS2-YFP-CcrM	replicating vector expressing YFP-CcrM under the control of P_{xyl}	This study
pMCS6-DnaAlocus-PdnaA-CYPF	integrating vector harboring P_{dnaA}-CYFP reporter cassette and a *dnaA* integration site	This study
pMCS6-DnaAlocus-PctrA1-CYPF	integrating vector harboring P_{ctrA1}-CYFP reporter cassette and a *dnaA* integration site	This study
pMCS6-TrpElocus-PdnaA-CYPF	integrating vector harboring P_{dnaA}-CYFP reporter cassette and a *trpE* integration site	This study
pMCS6-TrpElocus-PctrA1-CYPF	integrating vector harboring P_{ctrA1}-CYFP reporter cassette and a *trpE* integration site	This study
pMCS2-mopJ	to generate *ΔmopJ*	This study
pMCS2-spmX	to generate *ΔspmX*	This study
pMCS2-perP	to generate *ΔperP*	This study
pMCS2-podJ	to generate *ΔpodJ*	This study

References

1. Gur E, Sauer RT (2009) Degrons in protein substrates program the speed and operating efficiency of the AAA+ Lon proteolytic machine. *Proc Natl Acad Sci U S A* 106(44):18503–8.

2. Ward D, Newton A (1997) Requirement of topoisomerase IV parC and parE genes for cell cycle progression and developmental regulation in Caulobacter crescentus. *Mol Microbiol* 26(5):897–910.

3. Karlowicz A, et al. (2017) Defining the crucial domain and amino acid residues in bacterial Lon protease for DNA binding and processing of DNA-interacting substrates. *J Biol Chem* 292(18):7507–7518.

4. Schrader JM, Shapiro L (2015) Synchronization of Caulobacter Crescentus for Investigation of the Bacterial Cell Cycle. *J Vis Exp* (98). doi:10.3791/52633.

5. Wienken CJ, Baaske P, Rothbauer U, Braun D, Duhr S (2010) Protein-binding assays in biological liquids using microscale thermophoresis. *Nat Commun* 1(7):100.

6. Schmittgen TD, Livak KJ (2008) Analyzing real-time PCR data by the comparative CT method. *Nat Protoc* 3(6):1101–1108.

7. Bayas CA, et al. (2018) Spatial organization and dynamics of RNase E and ribosomes in Caulobacter crescentus. *Proc Natl Acad Sci U S A* 115(16):E3712–E3721.

8. Gahlmann A, et al. (2013) Quantitative Multicolor Subdiffraction Imaging of Bacterial Protein Ultrastructures in Three Dimensions. *Nano Lett* 13(3):987–993.

9. Lam H, Schofield WB, Jacobs-Wagner C (2006) A landmark protein essential for establishing and perpetuating the polarity of a bacterial cell. *Cell* 124(5):1011–23.

10. Iniesta AA, Hillson NJ, Shapiro L (2010) Cell pole-specific activation of a critical bacterial cell cycle kinase. *Proc Natl Acad Sci U S A* 107(15):7012–7.

11. Bowman GR, et al. (2008) A Polymeric Protein Anchors the Chromosomal Origin/ParB Complex at a Bacterial Cell Pole. *Cell* 134(6):945–955.

12. Thanbichler M, Iniesta AA, Shapiro L (2007) A comprehensive set of plasmids for vanillate- and xylose-inducible gene expression in Caulobacter crescentus. *Nucleic Acids Res* 35(20):e137.